



## NEUROSCIENCE

# Antagonism of $\beta$ -arrestins in IL-4-driven microglia reactivity via the Samd4/mTOR/OXPHOS axis in Parkinson's disease

Jiaqi Liu<sup>1</sup>, Yue Liang<sup>1</sup>, Qinghao Meng<sup>1</sup>, Jiayu Chen<sup>2</sup>, Junwei Ma<sup>2</sup>, Hong Zhu<sup>1</sup>, Lei Cai<sup>2</sup>, Nanshan Song<sup>2</sup>, Jianhua Ding<sup>1</sup>, Yi Fan<sup>1</sup>, Ming Lu<sup>1</sup>, Guangyu Wu<sup>3</sup>, Yinquan Fang<sup>1\*</sup>, Gang Hu<sup>1,2\*</sup>

Interleukin-4 (IL-4)-exposed microglia acquire neuroprotective properties, but their functions and regulation in Parkinson's disease (PD) are poorly understood. In this study, we demonstrate that IL-4 enhances anti-inflammatory microglia reactivity, ameliorates the pathological features of PD, and reciprocally affects expression of  $\beta$ -arrestin 1 and  $\beta$ -arrestin 2 in microglia in PD mouse models. We also show that manipulation of two  $\beta$ -arrestins produces contrary effects on the anti-inflammatory states and neuroprotective action of microglia induced by IL-4 in vivo and in vitro. We further find that the functional antagonism of two  $\beta$ -arrestins is mediated through sequential activation of sterile alpha motif domain containing 4 (Samd4), mammalian target of rapamycin (mTOR), and mitochondrial oxidative phosphorylation (OXPHOS). Collectively, these data reveal opposing functions of two closely related  $\beta$ -arrestins in regulating the IL-4-induced microglia reactivity via the Samd4/mTOR/OXPHOS axis in PD mouse models and provide important insights into the pathogenesis and therapeutics of PD.

## INTRODUCTION

Parkinson's disease (PD) is one of the most common movement disorders and the second most common neurodegenerative diseases (1). With the increased longevity, PD prevalence increases rapidly at a rate faster than other neurological disorders (1, 2). Although the etiologies of PD are complex involving genetic, epigenetic, and environmental factors (3), neuroinflammation and the degeneration of dopaminergic (DA) neurons in the substantia nigra pars compacta (SNc) are two of the pathological hallmarks of PD (2, 4).

Microglia are brain-resident immune cells that play an important role in the homeostasis of the central nervous system (CNS) (5). Emerging evidence suggests that they are the key cell types associated with the pathogenesis of PD (4, 6–9) and targeting their reactivity is regarded as a therapeutic approach of PD. However, therapeutic effects of general immune-suppressive drugs that control microglial activation are limited, especially in clinic studies (10). In addition to the neurotoxic effects, hyperreactive microglia may have protective actions on the viability and function of neurons (11–13).

Interleukin-4 (IL-4) is a multifunctional cytokine and a key regulator in humoral and adaptive immunity (14). It is also expressed in the brain and regulates the physiological functions of the CNS. Numerous studies have shown that IL-4 exposure induces anti-inflammatory and neurotrophic states of microglia (14–17) and that enhanced IL-4 expression produces neuroprotective and neuroregenerative benefits in the experimental models of CNS diseases, including depression, multiple sclerosis, stroke, spinal cord injury, and neuropathic pain (15, 18–21). IL-4 is increased in peripheral blood and ventricular cerebrospinal fluid in patients with PD (22, 23). However, the functions and regulation of IL-4-induced microglia in PD remain largely undefined.

$\beta$ -Arrestins (ARRBs) have two isoforms, ARRB1 and ARRB2 (also known as arrestin-2 and arrestin-3, respectively), both are originally identified as key mediators for the internalization and trafficking of G protein-coupled receptors (GPCRs) (24–26). It is now well recognized that they are important signal transducers in multiple signaling cascades that may be independent of GPCRs (27, 28). Although structurally closely related, they may regulate distinct or even contrary cellular processes (29, 30). For example, ARRB1 knockout (KO) alleviates, whereas ARRB2 KO exacerbates, the symptoms of experimental autoimmune encephalomyelitis mouse models (31, 32). Our previous studies suggest that ARRB1 and ARRB2 play distinct roles in microglia-mediated inflammation (33). However, nothing is known about their functions in microglia-mediated neuroprotection.

In this study, we have demonstrated that IL-4 overexpression in the midbrain induces anti-inflammatory microglia reactivity, ameliorates movement impairments, DA neuron loss, and neuroinflammation, and reverses the unbalanced expression of microglial ARRB1 and ARRB2 in PD mouse models. We have also shown that ARRB1 and ARRB2 inversely affect the induction and neuroprotective effects of anti-inflammatory microglia induced by IL-4, which is mediated through the sterile alpha motif domain containing 4 (Samd4), mammalian target of rapamycin (mTOR), and mitochondrial oxidative phosphorylation (OXPHOS). Our work identifies the therapeutic roles and regulation of IL-4-driven microglia in PD and suggests a potential therapeutic strategy for PD.

## RESULTS

## IL-4 overexpression in the midbrain alleviates PD-like motor symptoms, DA neuron loss, and neuroinflammation in vivo

To define the role of IL-4 in the 1-methyl-4-phenyl-1,2,3,6-tetraphydropyridine (MPTP)-induced PD mouse model, we used adeno-associated viruses (AAVs) to increase IL-4 expression specifically in the midbrain (Fig. 1A) as confirmed by immunoblotting (Fig. 1, B and C). MPTP challenge increased total time in the pole test (Fig. 1D) but decreased the latency time in the rotarod test (Fig. 1E) and the movement speed of mice in the open field test (OFT) (Fig. 1, F and G), all of which

<sup>1</sup>Jiangsu Key Laboratory of Neurodegeneration, Department of Pharmacology, School of Basic Medical Sciences, Nanjing Medical University, 818 Tianyuan East Road, Nanjing, Jiangsu 211166, China. <sup>2</sup>Department of Pharmacology, Nanjing University of Chinese Medicine, 138 Xianlin Avenue, Nanjing, Jiangsu 210023, China. <sup>3</sup>Department of Pharmacology and Toxicology, Medical College of Georgia, Augusta University, 1459 Laney Walker Blvd., Augusta, GA 30912, USA.

\*Corresponding author. Email: ghu@njmu.edu.cn (G.H.); fangyinquan26@njmu.edu.cn (Y. Fang)

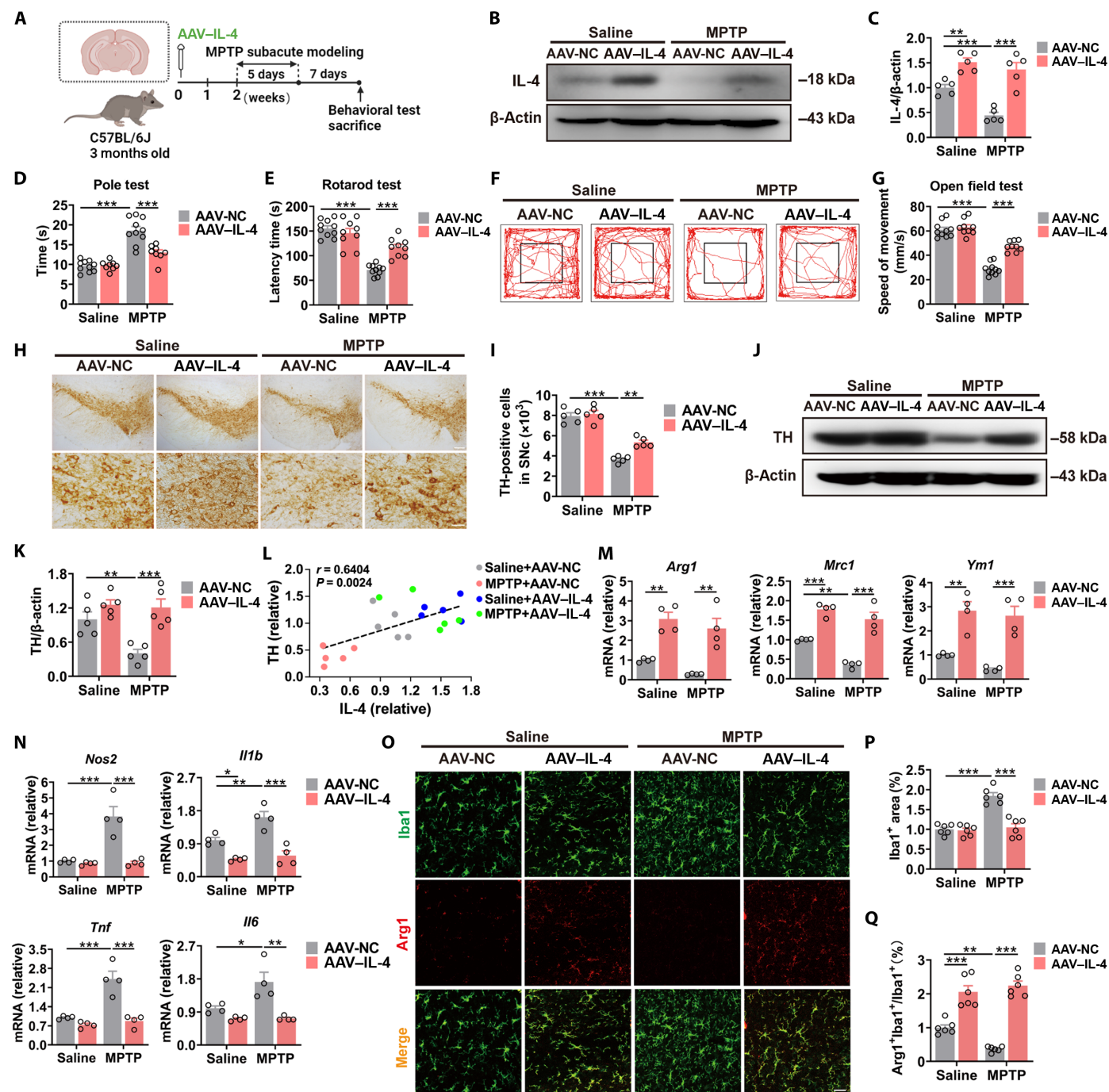


**Fig. 1. IL-4 overexpression in the midbrain alleviates motor impairments, DA neuron loss, and neuroinflammation in PD models.** (A) Schematic diagram of AAV injection and MPTP subacute model preferment. Behavioral tests and biochemical analysis were then conducted. (B) IL-4 expression in the midbrain of MPTP-induced PD mouse models. (C) Quantitative data shown in (B) ( $n = 5$ ). (D) The total time in the pole test ( $n = 8$  to 10). (E) The latency time in the rotarod test ( $n = 9$  to 10). (F and G) The circuit diagram (F) and the movement speed of mice (G) in the OFT ( $n = 9$  to 10). (H and I) Immunohistochemistry (H) and stereological counts (I) of TH<sup>+</sup> DA neuron in the SNc of MPTP-induced PD mice ( $n = 5$ ). Scale bars, 200  $\mu$ m (top) or 40  $\mu$ m (bottom). (J) The protein levels of TH in the midbrain of mice after MPTP stimulation. (K) Quantitative data shown in (J) ( $n = 5$ ). (L) Correlation between the protein levels of TH and IL-4 in the midbrain of MPTP-induced PD models ( $n = 5$ ). (M and N) mRNA levels of anti- and proinflammatory markers in the midbrain of PD mice after AAV injection ( $n = 4$ ). (O and Q) Arg1 expression on Iba1<sup>+</sup> microglia in the SNc of mice after MPTP stimulation ( $n = 6$ ). Scale bar, 50  $\mu$ m. (P) Quantitative data showing fluorescence area of Iba1<sup>+</sup> microglia in (O) ( $n = 6$ ). Quantitative data are means  $\pm$  SE. \* $P < 0.05$ , \*\* $P < 0.01$ , and \*\*\* $P < 0.001$ .

were inhibited by IL-4 overexpression in the midbrain (Fig. 1, D to G). Moreover, IL-4 overexpression normalized the reduction of DA neurons in the SNc and tyrosine hydroxylase (TH) protein levels in the midbrain of mice after MPTP treatment as measured by antibody staining (Fig. 1, H and I) and immunoblotting (Fig. 1, J and K). Correlation analysis showed that IL-4 expression in the midbrain positively correlated with the TH concentration (Fig. 1L), suggesting that the DA neuron viability is associated with the expression levels of IL-4 in the midbrain.

We then determined the effects of IL-4 on neuroinflammation. AAV-mediated IL-4 expression significantly enhanced the levels of anti-inflammatory markers, including *Arg1*, *Ym1*, and *Mrc1* genes, and reduced the levels of proinflammatory markers, including *Il6*, *Il1b*, *Tnfa*, and *Nos2* genes, in MPTP-stimulated mouse midbrain (Fig. 1, M and N). As arginase 1 (*Arg1*) is one of the most recognized markers of anti-inflammatory microglia (34), double immunofluorescence staining was used to quantify *Arg1* expression and anti-inflammatory microglia reactivity in the midbrain using ionized calcium-binding adapter molecule 1 (*Iba1*) as a microglia marker. The expression of *Iba1* was increased in the SNc of MPTP-induced PD mice, and this increase was attenuated by AAV-mediated IL-4 expression (Fig. 1, O and P). In addition, the proportion of *Arg1*<sup>+</sup> microglia was significantly elevated by AAV-mediated IL-4 expression in the SNc of mice under both saline and MPTP treatments (Fig. 1, O and Q). These results suggest that IL-4 overexpression in the midbrain enhances anti-inflammatory microglia reactivity and alleviates PD-like motor impairments and DA neuron loss in vivo.

### IL-4 differentially regulates the expression of two ARRBs in PD mouse models

As our previous study has shown that the relative expression of ARRB1 and ARRB2 in microglia controls the inflammatory responses of microglia and the pathogenesis of PD (33), we measured their expression in the midbrain of PD mice after IL-4 overexpression. As expected, ARRB1 expression was increased, whereas ARRB2 was decreased, in MPTP-stimulated mouse midbrain, both of which were reversed by AAV-mediated IL-4 expression (Fig. 2, A and B). IL-4 overexpression also abolished the enhancement of ARRB1 and the reduction of ARRB2 in microglia in the SNc of MPTP-induced PD mice (Fig. 2, C to F). In contrast, IL-4 overexpression and MPTP stimulation did not alter the expression of ARRB1 in astrocytes (fig. S1). Consistent with their expression in PD models in vivo, ARRB1 expression was attenuated, whereas ARRB2 expression was augmented in primary cultures of microglia after IL-4 stimulation (fig. S2). Correlation analysis showed that ARRB1 and IL-4 expression levels in the midbrain were negatively correlated, whereas the correlation between ARRB2 and IL-4 protein levels was positive (Fig. 2G). Similarly, opposite correlation was observed between two ARRBs with TH expression and the numbers of DA neurons and *Arg1*<sup>+</sup> microglia in the midbrain and microglia (Fig. 2, H to J). These data suggest that the actions of IL-4 overexpression in mouse models of PD may be attributable to differential expression of ARRB1 and ARRB2.

### Microglial ARRBs contrarily regulate the neuroprotective functions of IL-4 in PD mouse models

We then determined the effects of microglial ARRBs on the functions of IL-4 in the MPTP-induced PD mouse model. As our preceding data have shown that IL-4 overexpression causes ARRB1 down-regulation and ARRB2 up-regulation in microglia, AAVs carrying the microglia-specific promoter F4/80 were used to deliver

plasmids or small interfering RNA (siRNA) to manipulate the expression of ARRBs in microglia (Fig. 3A and fig. S3). As measured in rotarod test, pole test, and OFT, the improvement of motor behaviors in MPTP-stimulated mice by IL-4 treatment was blocked by either ARRB1 overexpression or ARRB2 knockdown in microglia (Fig. 3, B to E). ARRB1 overexpression or ARRB2 knockdown in microglia also abolished the protective effects of IL-4 on DA neuron loss in the midbrain of MPTP mouse models (Fig. 3, F to I) and suppressed the functions of IL-4 in the induction of anti-inflammatory microglia reactivity and in the inhibition of proinflammatory responses in PD mice (Fig. 3, J to M).

To define whether microglial ARRBs mediated the neuroprotective effects of IL-4 in vitro, we measured the effects of conditioned medium (CM) collected from microglia with or without IL-4 treatment on primary ventral mesencephalon (VM) neurons after 1-methyl-4-phenylpyridinium (MPP)<sup>+</sup> stimulation in vitro (Fig. 4A). The CM from microglia treated with IL-4 markedly enhanced the viability of the neurons (Fig. 4B) and reduced the release of lactate dehydrogenase (LDH) in the supernatant of neurons (Fig. 4C) after MPP<sup>+</sup> treatment for 24 hours. The neurons exhibited apoptotic features, including chromatin condensation, nuclear fragmentation, and impaired neurite length upon MPP<sup>+</sup> stimulation, which were inhibited by the CM from microglia treated with IL-4 (Fig. 4, D to G). All of these protective effects were potentiated by ARRB1 KO (fig. S4A) but mitigated by ARRB2 KO (fig. S4B) in microglia (Fig. 4, B to G). These results suggest that microglial ARRB1 and ARRB2 play contradictory roles in the neuroprotective action of IL-4-driven microglia in PD mouse models in vivo and in vitro.

### Two ARRBs exert opposing roles in the anti-inflammatory states in primary cultured cells

To further measure the effects of ARRBs in IL-4-driven microglia, we used the loss- and gain-of-function approaches. In the loss-of-function studies, ARRB1 ablation significantly enhanced, whereas ARRB2 ablation inhibited the expression of the anti-inflammatory marker CD206 (encoded by *Mrc1*) and genes (*Arg1*, *Ym1*, and *Mrc1*) in microglia after IL-4 treatment (Fig. 5, A to C and E to G). In the gain-of-function studies, ARRB1 overexpression (fig. S5) significantly reduced, whereas ARRB2 overexpression (fig. S5) promoted the transcription of anti-inflammatory markers in microglia (Fig. 5, D and H).

As IL-4 also stimulates anti-inflammatory properties in macrophages (19, 35), bone marrow-derived macrophages (BMDMs) were used to confirm the effects of ARRBs on microglia. ARRB1 KO enhanced the expression of anti-inflammatory marker genes and CD206, and the release of anti-inflammatory cytokines (IL-10 and transforming growth factor- $\beta$ ) in BMDMs after IL-4 stimulation (fig. S6, A to D). Immunofluorescence imaging showed that CD206 expression in BMDMs was increased by ARRB1 KO upon IL-4 stimulation (fig. S6, E and F). In contrast, ARRB2 KO reduced the expression and secretion of anti-inflammatory markers in BMDMs after IL-4 treatment (fig. S6, G to L).

As the signal transducers and activators of transcription 6 (STAT6) pathway is important for IL-4-mediated anti-inflammatory states in both microglia and macrophage (19), we investigated whether ARRB1 and ARRB2 could regulate this pathway. ARRB1 KO significantly stimulated, whereas ARRB2 KO inhibited STAT6 activation (fig. S6, M to P). These data demonstrate that ARRB1 and ARRB2 oppositely regulate the IL-4-induced anti-inflammatory reactive states of microglia and macrophages.

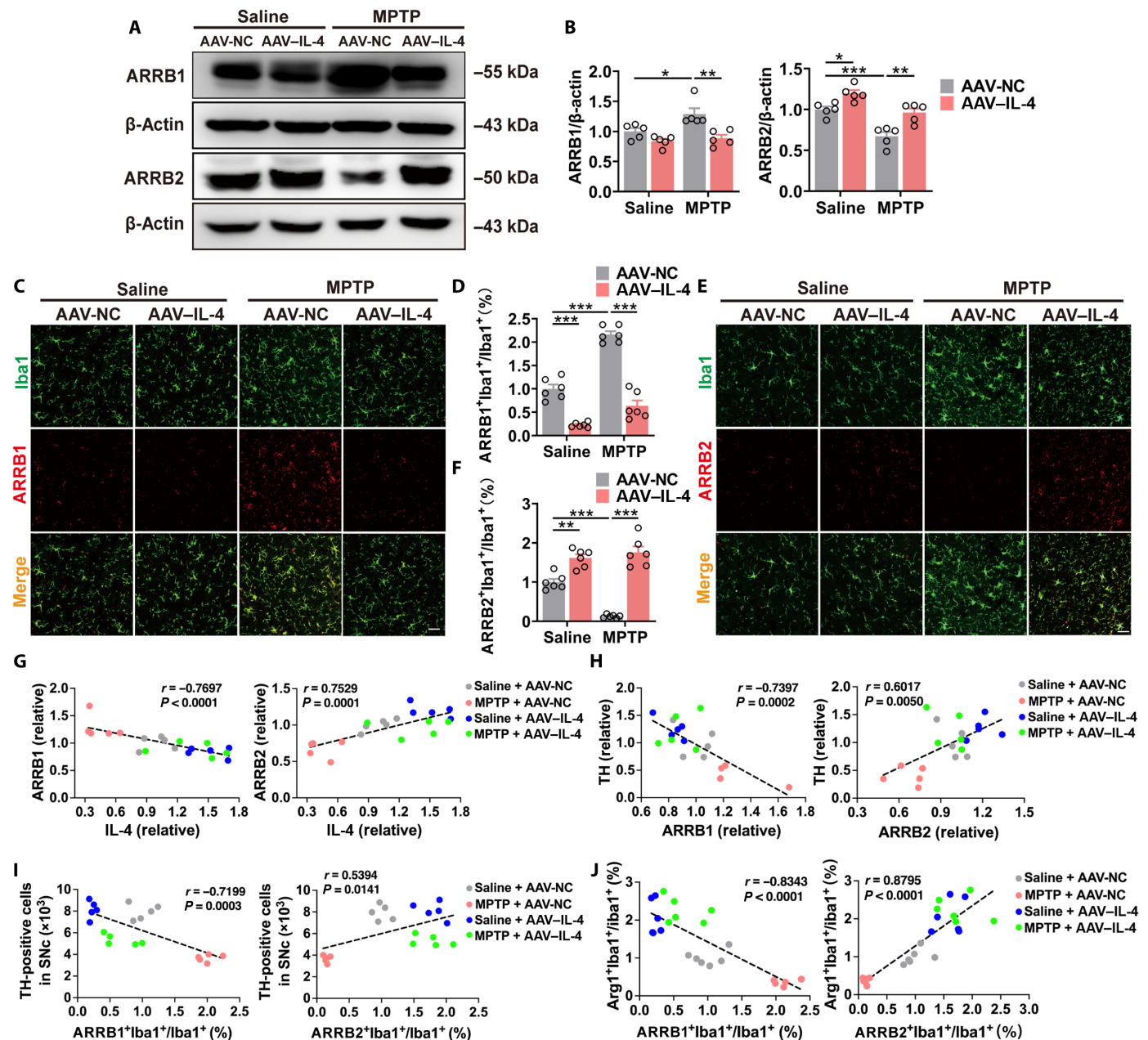


**Fig. 2. IL-4 differentially regulates the expression of ARRB1 and ARRB2 in PD mouse models.** (A) The protein levels of ARRB1 and ARRB2 in the midbrain of PD mice after AAV injection. (B) Quantitative data shown in (A) ( $n = 5$ ). (C to F) Expression of ARRB1 [(C) and (D)] and ARRB2 [(E) and (F)] in microglia in the SNc of MPTP-induced PD models ( $n = 6$ ). Scale bars, 50  $\mu$ m. (G) Correlation between the protein levels of ARRB1 or ARRB2 and IL-4 in the midbrain ( $n = 5$ ). (H) Correlation between the expression of TH and ARRB1 or ARRB2 in the midbrain ( $n = 5$ ). (I) Correlation between the numbers of DA neuron and ARRB1<sup>+</sup> or ARRB2<sup>+</sup> microglia in the SNc ( $n = 5$ ). (J) Correlation between the levels of Arg1<sup>+</sup> and ARRB1<sup>+</sup> or ARRB2<sup>+</sup> microglia in the SNc ( $n = 6$ ). Quantitative data are means  $\pm$  SE. \* $P < 0.05$ , \*\* $P < 0.01$ , and \*\*\* $P < 0.001$ .

### Mitochondrial OXPHOS mediates the effects of ARRBs on IL-4-induced microglia reactivity

As the anti-inflammatory properties of microglia rely on mitochondrial OXPHOS (36), we measured the oxygen consumption rate (OCR) in wild-type (WT) and ARRB KO microglia using the Seahorse XF96 analyzer. IL-4 treatment slightly enhanced the basal and maximal respiration of OCR in microglia, and this effect was further elevated by ARRB1 KO but inhibited by ARRB2 KO (Fig. 6, A to D).

siRNA-mediated ARRB1 knockdown (fig. S7) and transient expression of ARRB2 increased the expression of anti-inflammatory markers at the mRNA levels (*Arg1*, *Mrc1*, and *Ym1*) and protein levels (Arg1 and CD206) in microglia after IL-4 stimulation, and these effects were blocked by pretreatment with the mitochondrial electron chain inhibitor oligomycin (Fig. 6, E to J). These results suggest an important role of mitochondrial OXPHOS in mediating the functions of ARRBs in anti-inflammatory microglia reactivity.

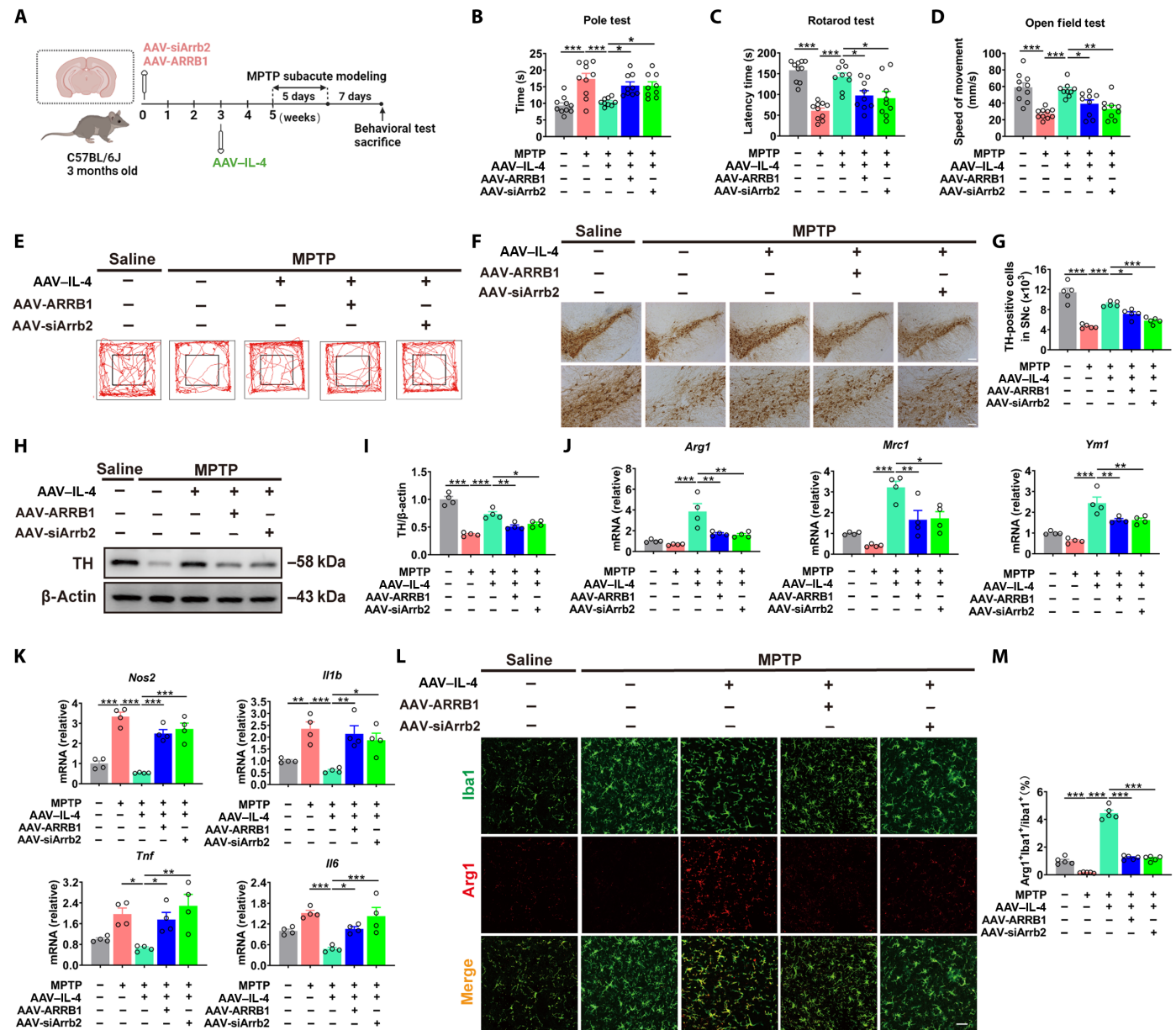


**Fig. 3. Microglial ARRBs contrarily regulate the neuroprotective functions of IL-4 in PD mouse models.** (A) Schematic diagram of AAV injection and MPTP subacute model preferment. Behavioral tests and biochemical analysis were then conducted. (B) The total time in the pole test ( $n = 9$  to  $10$ ). (C) The latency time in the rotarod test ( $n = 9$  to  $10$ ). (D and E) The movement speed of mice (D) and the circuit diagram (E) in the OFT ( $n = 9$  to  $10$ ). (F and G) Immunohistochemistry (F) and stereological counts (G) of TH<sup>+</sup> DA neuron in the SNc of MPTP-induced PD models ( $n = 5$ ). Scale bars, 200  $\mu$ m (top) or 50  $\mu$ m (bottom). (H) The protein levels of TH in the midbrain of PD mice after AAV injection. (I) Quantitative data shown in (H) ( $n = 4$ ). (J and K) mRNA levels of anti- and proinflammatory markers in the midbrain of PD mice after AAV injection ( $n = 4$ ). (L and M) Arg1 expression in microglia in the SNc of MPTP-induced PD models ( $n = 5$ ). Scale bar, 50  $\mu$ m. Quantitative data are means  $\pm$  SE. \* $P < 0.05$ , \*\* $P < 0.01$ , and \*\*\* $P < 0.001$ .

### Samd4 is a previously unknown effector of ARRBs in IL-4-driven microglia

To elucidate the molecular mechanisms underlying the functions of ARRBs, we performed RNA sequencing (RNA-seq) to identify the genes that were differentially expressed in WT and *Arrb2*<sup>-/-</sup> microglia in response to IL-4 (fig. S8A). This strategy identified 334 genes that were up-regulated and 157 genes that were down-regulated in

*Arrb2*<sup>-/-</sup> microglia (fig. S8B). Analysis of the enriched Kyoto Encyclopedia of Genes and Genomes pathways showed that these up-regulated genes were associated with inflammatory and cytokine responses (fig. S8C).

As compared with WT microglia, 15 inflammation-related genes (*Cd5l*, *Pttg1*, *Samd4*, *Nes*, *Tmem100*, *Spp1*, *S100a10*, *Gpat3*, *Tom1l1*, *Serpinb2*, *Pml*, *Il12rb1*, *Mag*, *Aebp1*, and *Mmp3*) were clearly changed in

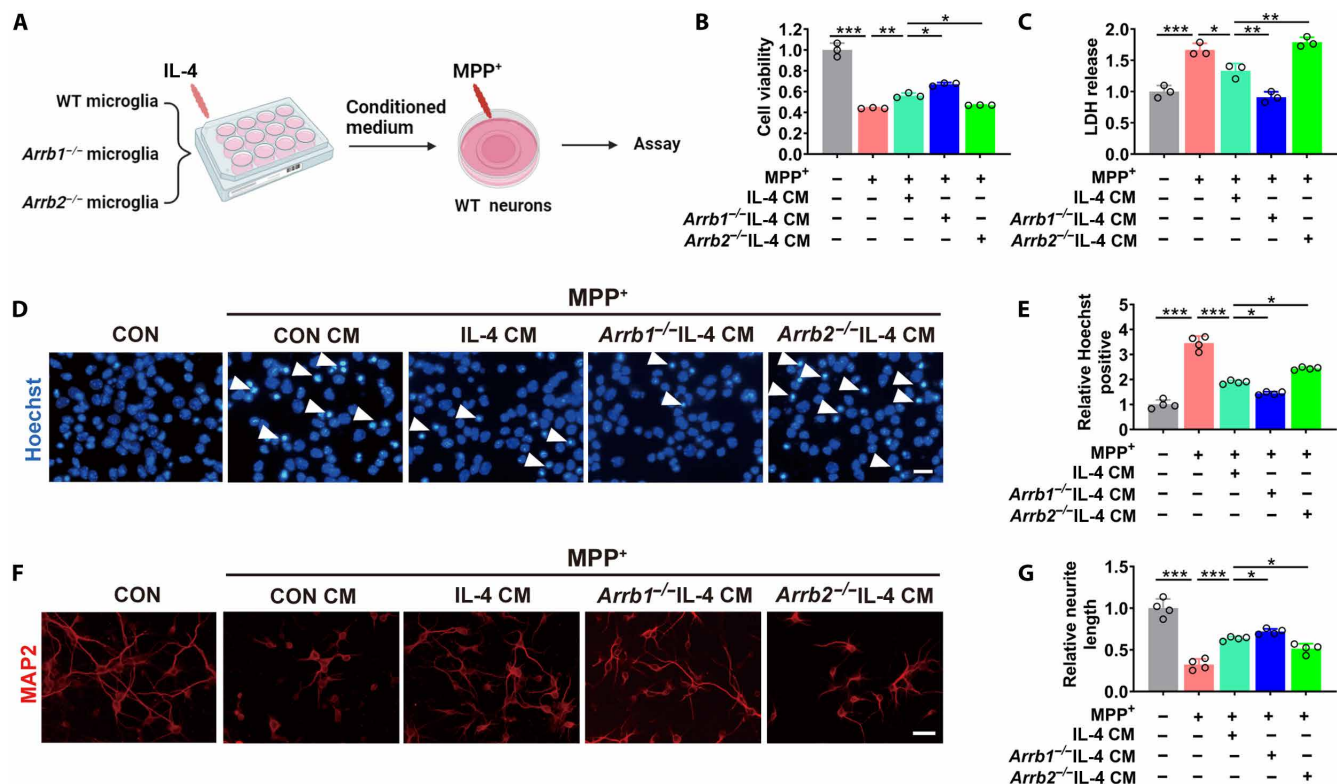


**Fig. 4. Opposing roles of microglial ARRB1 and ARRB2 in the neuroprotective functions of IL-4 in primary neurons.** (A) Schematic diagram showing the treatment of primary neurons isolated from wild-type (WT) mice with CMs of WT, ARRB1, or ARRB2 KO microglia with or without MPP<sup>+</sup> stimulation for 24 hours. (B) The viability of VM neurons. (C) The releases of LDH in the supernatants of neurons. (D and E) Nuclear morphology (D) and Hoechst-positive neurons (E). Arrowheads indicate Hoechst-positive nuclei. Scale bar, 20 μm. (F and G) Morphology of VM neurons (F) and MAP2<sup>+</sup> cell neurite length (G). Scale bar, 40 μm. Quantitative data are means ± SE. (n = 3 to 4). \*P < 0.05, \*\*P < 0.01, and \*\*\*P < 0.001.

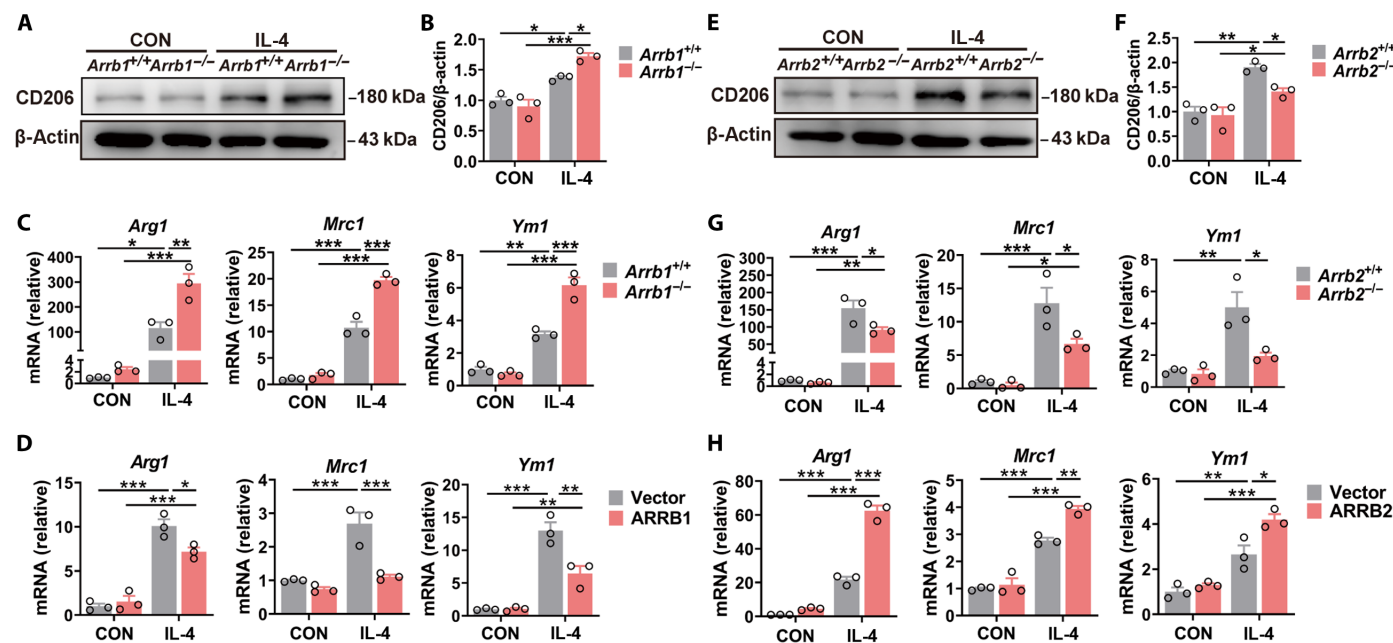


**Fig. 5. Two ARRBs produce opposing roles in the anti-inflammatory states in primary cultured cells.** (A, B, E, and F) CD206 expression in ARRB1 [(A) and (B)] and ARRB2 [(E) and (F)] KO primary culture microglia after IL-4 stimulation for 24 hours. (C and G) Levels of anti-inflammatory gene transcripts in ARRB1 (C) and ARRB2 (G) KO microglia after IL-4 treatment for 6 hours. (D and H) Anti-inflammatory gene expression in microglia transfected with ARRB1 (D) or ARRB2 (H) after IL-4 treatment for 6 hours. Quantitative data are means ± SE (n = 3). \*P < 0.05, \*\*P < 0.01, and \*\*\*P < 0.001.

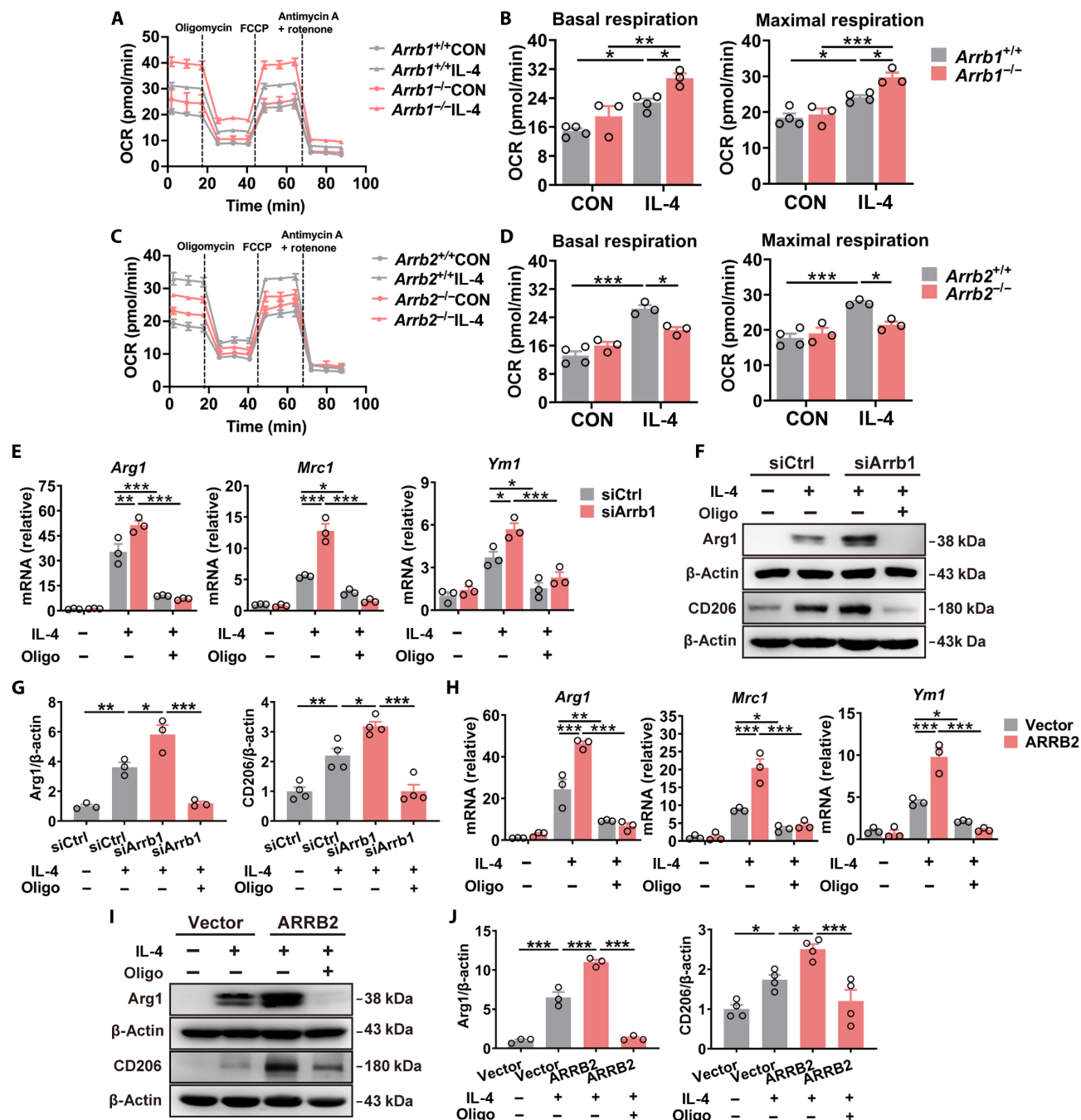


**Fig. 6. Mitochondrial OXPHOS mediates the differential roles of ARRBs in anti-inflammatory microglia reactivity.** (A to D) OCR changes in ARRB1 [(A) and (B)] and ARRB2 [(C) and (D)] KO microglia after IL-4 stimulation for 24 hours. [(B) and (D)] Quantification of basal and maximal respiratory capacity. (E and H) Levels of anti-inflammatory gene transcripts in microglia transfected with *Arrb1* siRNA (E) and *ARRB2* plasmids (H) after IL-4 stimulation with or without oligomycin (Oligo; 2  $\mu$ M) pretreatment. (F, G, I, and J) The protein levels of Arg1 and CD206 in ARRB1 knockdown [(F) and (G)] and ARRB2 overexpression [(I) and (J)] in microglia after IL-4 treatment with or without oligomycin pretreatment. Quantitative data shown in (H) and (J). Quantitative data are means  $\pm$  SE ( $n = 3$  to 4). \* $P < 0.05$ , \*\* $P < 0.01$ , and \*\*\* $P < 0.001$ .

*Arrb2*<sup>-/-</sup> microglia in the RNA-seq data (fig. S8D), and these changes were confirmed by reverse transcription quantitative polymerase chain reaction (RT-qPCR) (fig. S8E). Among the 15 genes, only *Samd4* was decreased by ARRB2 KO but increased by ARRB1 KO in microglia after IL-4 treatment (Fig. 7, A and B, and fig. S8, E and F). The same results were observed for *Samd4* expression at the protein levels in ARRB1 and

ARRB2 KO microglia (Fig. 7, C to F). Consistent with the data obtained from cell cultures in vitro, ARRB1 overexpression or ARRB2 knock-down in microglia significantly reduced the mRNA level of *Samd4* in the midbrain of MPTP-induced mice after IL-4 overexpression (fig. S9).

We next determined whether manipulation of *Samd4* expression in ARRB1 and ARRB2 KO microglia could affect the functions of

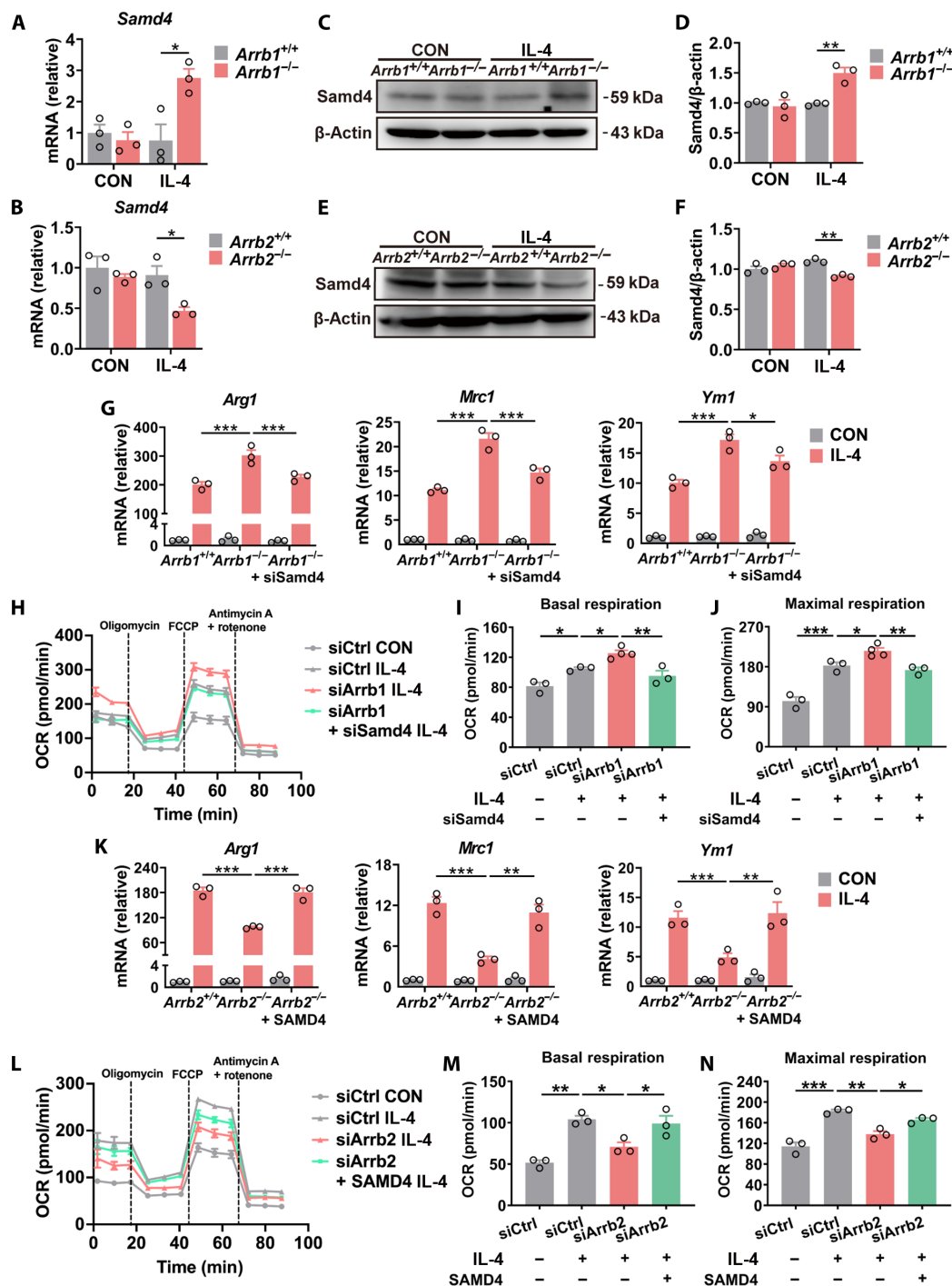


**Fig. 7. Samd4 is a previously unknown effector of ARRBs in IL-4-driven microglia.** (A and B) mRNA levels of *Samd4* in ARRB1 (A) and ARRB2 (B) KO microglia after IL-4 stimulation for 6 hours. (C to F) The protein levels of *Samd4* in ARRB1 [(C) and (D)] and ARRB2 [(E) and (F)] KO microglia after IL-4 treatment for 24 hours. Quantitative data shown in (D) and (F). (G) Anti-inflammatory gene expression in microglia from WT and ARRB1 KO mice after transfection with *Samd4* siRNA for 48 hours. (H to J) OCR changes in BV-2 microglia transfected with *Arrb1* and *Samd4* siRNA after IL-4 stimulation for 24 hours. [(I) and (J)] Quantification of basal and maximal respiratory capacity. (K) Levels of anti-inflammatory gene transcripts in microglia from WT and ARRB2 KO mice after transfection with *Samd4* plasmids. (L to N) OCR changes in BV-2 microglia transfected with *Arrb2* siRNA and S*AMD4* plasmids after IL-4 stimulation for 24 hours. [(M) and (N)] Quantification of basal and maximal respiratory capacity. Quantitative data are means  $\pm$  SE ( $n = 3$ ). \* $P < 0.05$ , \*\* $P < 0.01$ , and \*\*\* $P < 0.001$ .

ARRBs in IL-4-induced microglia. *Samd4* knockdown by siRNA in ARRB1 KO microglia (fig. S10, A and B) inhibited (Fig. 7G), whereas *Samd4* overexpression (fig. S10, C and D) in ARRB2 KO microglia enhanced (Fig. 7K), the expression of anti-inflammatory marker genes after IL-4 treatment. ARRB1 knockdown stimulated the basal and maximal respiration of OCR in BV-2 microglia cells treated with IL-4, and this effect was reversed by *Samd4* knockdown (Fig. 7, H to J). ARRB2 knockdown inhibited the basal and maximal respiration of OCR in BV-2 microglia cells treated with IL-4, which was reversed by *Samd4* overexpression (Fig. 7, L to N). These data suggest that *Samd4* is an effector, acting downstream of both ARRBs and mediating their differential functions in anti-inflammatory reactive states of microglia.

### The mTOR pathway acts downstream of *Samd4* in the functional antagonism of ARRBs in anti-inflammatory microglia reactivity

As *Samd4* mediates the mTORC1 signaling (37), we determined the effects of ARRBs on the activation of mTOR and its downstream molecule p70 S6 kinase (p70S6k) in microglia. The activation of mTOR and p70S6k was not changed in ARRB1 and ARRB2 KO microglia as compared with WT microglia at the basal level. However, their activation in response to IL-4 treatment was enhanced by ARRB1 KO but impaired by ARRB2 KO (Fig. 8, A to D). Furthermore, *Samd4* knockdown in ARRB1 KO microglia inhibited, whereas *Samd4* overexpression in ARRB2 KO microglia promoted their activation after IL-4 treatment (Fig. 8, E to H).

We next used pharmacological inhibitors to further determine the role of the mTOR pathway in ARRB-mediated anti-inflammatory microglia reactivity. The pretreatment with the mTORC1 inhibitor rapamycin decreased the mRNA levels of anti-inflammatory markers, as well as the basal and maximal respiration of OCR, in ARRB1 KO microglia after IL-4 stimulation (Fig. 8, I, K, and L), whereas the pretreatment with the mTOR activator MHY1485 reversed the effects of IL-4 in ARRB2 KO microglia (Fig. 8, J, M, and N). These results suggest that the mTOR pathway acts downstream of *Samd4* to mediate the effects of ARRBs in IL-4-induced anti-inflammatory microglia reactivity.

## DISCUSSION

This study has revealed opposing roles of ARRB1 and ARRB2 in regulating the induction and neuroprotective action of IL-4-driven microglia in PD mouse models (Fig. 9). We first demonstrated that IL-4 expression in the midbrain via AAVs induced anti-inflammatory reactivity of microglia and ameliorated motor dysfunction, DA neuron degeneration, and proinflammatory responses in PD mouse models, suggesting that the induction of IL-4-driven microglia is the promising treatment of PD. However, IL-4 treatment only partially protects against the loss of DA neurons in MPTP mouse models, which may be due to severe toxic effects of MPTP on neurons that could not be reversed by IL-4 and/or other factors involved. We further found that IL-4 normalized the expression of ARRB1 and ARRB2 in PD mouse models. Microglia-specific ARRB1 augmentation and ARRB2 depletion blocked anti-inflammatory microglia reactivity and neuroprotective effects induced by IL-4 both in vivo and in vitro, implying that the expression of individual ARRBs, as well as their expression ratio, in microglia is important in regulation of the IL-4-mediated beneficial microglia states in PD. On the basis of the data presented here, as well

as our previous studies (33), we can reasonably conclude that inhibiting the detrimental effects of ARRB1 and enhancing the beneficial effects of ARRB2 simultaneously are potential therapeutic interventions of PD.

Our data have demonstrated that ARRB1 and ARRB2 in microglia differentially regulate mitochondrial OXPHOS to affect anti-inflammatory microglia reactivity. Microglial programmed metabolic changes are involved in various cellular functions, including cytoskeletal changes, tissue remodeling, and cytokine synthesis in response to environmental stresses (38–40). Previous studies have found that the induction of microglial proinflammatory states relies on glycolysis and glutaminolysis, whereas anti-inflammatory microglia reactivity correlates with OXPHOS (41). Thus, the manipulation of metabolic reprogramming to alter reactive microglia states has the therapeutic potential for CNS diseases. Previous studies have also shown that ARRB1 mediates metabolic reprogramming from mitochondrial OXPHOS to glycolysis in gastric cancer cell (42), without knowing the role of ARRB2. Our data have shown the differential effects of ARRB1 and ARRB2 on OXPHOS and suggest a previously unappreciated function for ARRBs in regulating metabolic reprogramming of microglia.

We have found that *Samd4* is an important effector, acting downstream of ARRBs and upstream of mTOR in IL-4-driven microglia. RNA-seq analyses of genome-wide transcriptional profiles indicated that ARRBs differentially regulated *Samd4* expression in IL-4-treated microglia. We further confirmed that *Samd4* was the effector of ARRBs in anti-inflammatory microglia reactivity. *Samd4* is an RNA binding protein and participates in the stabilization, degradation, and translation repression of mRNA (43). As previous studies have mainly focused on its biological functions, its pathophysiological functions in various diseases still need further exploration (44). In addition, the interaction between *Samd4* and mTOR has been reported. For example, *Samd4* plays an important role in metabolic regulation through modulating mTORC1 signaling in muscle and adipose tissues (37). *Samd4A* is required for both mitochondrial respiration and morphology of the mitochondrial network that are also regulated by the adenosine 5'-monophosphate kinase–mTOR pathway (45). Our results suggest an integrated signaling pathway in which microglial ARRBs differently regulate anti-inflammatory microglia reactivity through controlling the *Samd4*/mTOR pathway activation, which, in turn, affects mitochondrial OXPHOS.

Our data showing the distinct expression patterns and functions of ARRB1 and ARRB2 in microglia are very interesting that extend our understanding on the functional antagonism of microglial ARRBs under the pathological and therapeutic environments. We have also found that ARRBs play contrary roles in both pro- and anti-inflammatory microglia reactivity through two different effectors, nitrogen permease regulator-like 3 and *Samd4*. Numerous studies have demonstrated that ARRB1 and ARRB2 may have distinct functions (29, 46). For example, selective depletion of ARRB2 in hepatocytes promotes hepatic glucagon receptor signaling, whereas ARRB1 depletion has no effects (47). ARRB1 KO in agouti-related protein neurons significantly impairs glucose tolerance and insulin sensitivity that are not affected by ARRB2 KO (30). In addition, ARRB1 and ARRB2 play differential roles in apoptosis through different signaling pathways (48, 49). Such a functional heterogeneity of the two ARRBs can be explained by their structural differences under distinct conditions as suggested recently (50).

Previous studies suggest that the expression levels of ARRBs are associated with pathology (27) and affected by different stimuli, such as

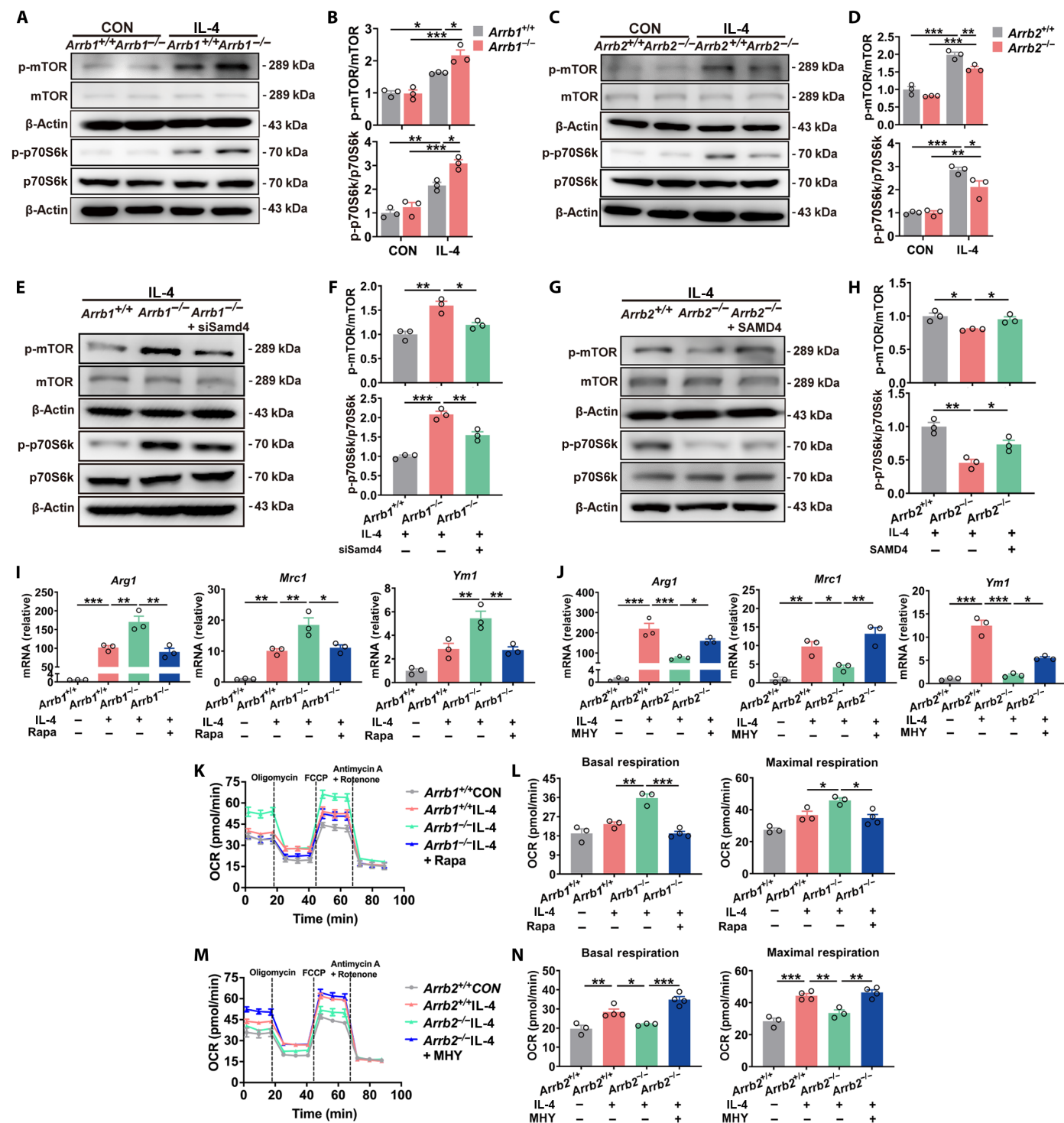


**Fig. 8. The mTOR pathway acts downstream of Samd4 in the contrarily effects of ARRBs on anti-inflammatory states of microglia.** (A to D) Activation of mTOR and p70S6k in ARR1 [(A) and (B)] or ARR2 [(C) and (D)] KO microglia with or without IL-4 stimulation. Quantitative data shown in (B) and (D). (E to H) The phosphorylation of mTOR and p70S6k in microglia from WT and ARRB KO mice transfected with either Samd4 siRNA for 48 hours [(E) and (F)] or SAMD4 plasmids [(G) and (H)] for 24 hours. Quantitative data shown in (F) and (H). (I and J) Levels of anti-inflammatory gene transcripts in microglia from WT and ARRB KO mice after IL-4 stimulation with or without rapamycin (Rapa) (I) or MHY1485 (MHY) (J) pretreatment. [(K) and (N)] Quantification of basal and maximal respiratory capacity. Quantitative data are means  $\pm$  SE (*n* = 3). \**P* < 0.05, \*\**P* < 0.01, and \*\*\**P* < 0.001.

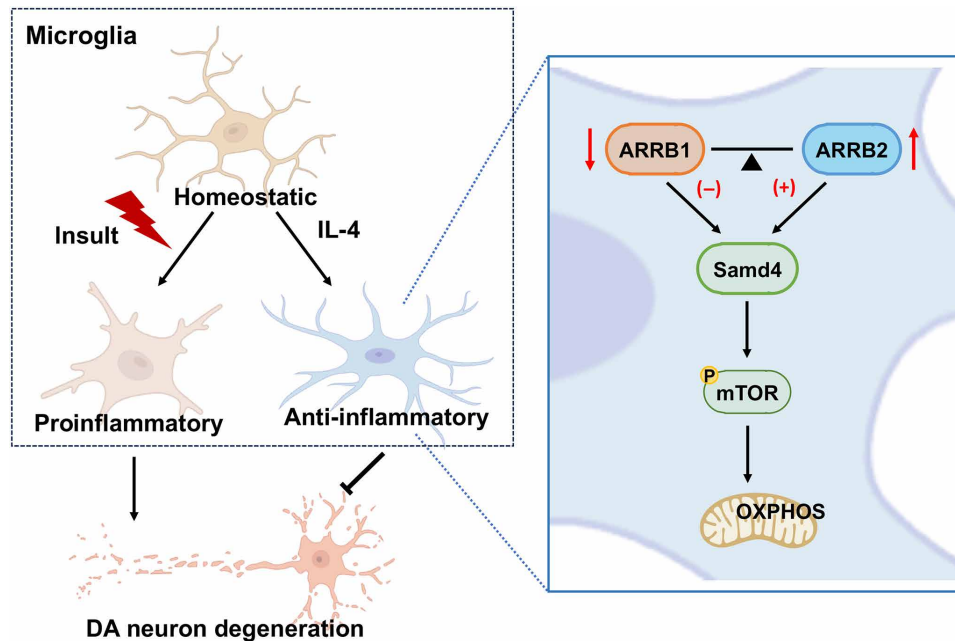


**Fig. 9. A schematic diagram showing the differential functions of ARR1 and ARR2 in the neuroprotection of IL-4-driven microglia in PD.** Microglia-mediated inflammation and DA neuron degeneration are alleviated by IL-4-induced anti-inflammatory microglia states in PD mouse models. IL-4 treatment decreases the expression of ARR1 but increases ARR2 in microglia. ARR1 inhibits, whereas ARR2 stimulates, the Samd4/mTOR/OXPHOS axis, leading to the enhancement of anti-inflammatory microglia reactivity. ↑, increased; ↓, decreased; +, stimulatory; −, inhibitory.

glucocorticoids (51), nuclear factor  $\kappa$ B (52), microRNAs (53–56), ethanol exposure (57), and antidepressants (58). The underlying mechanisms may involve transcriptional regulation, posttranslational modifications, or proteasomal degradation. Although we have demonstrated that IL-4 stimulation produces opposing effects on the expression of two ARR1 in microglia, the detailed mechanisms need further investigation.

In summary, we have revealed that ARR1 and ARR2 play important, but opposite, roles in IL-4-induced anti-inflammatory microglia reactivity and neuroprotection in PD mouse models that are mediated through the Samd4/mTOR/OXPHOS axis (Fig. 9). Our results provide important insights into the neuroprotective roles of IL-4 in PD through inducing anti-inflammatory states of microglia and may assist in the development of potential therapeutics for PD by targeting ARR1-mediated functional antagonism in microglia.

## MATERIALS AND METHODS

### Antibodies and reagents

All reagents, commercial kits, and antibodies are listed in table S1.

### Animals

C57BL/6J WT mice were purchased from the Animal Core Faculty of Nanjing Medical University. Arr1<sup>−/−</sup> mice were purchased from the Jackson Laboratory (Las Vegas, NV, strain: 011131), and Arr2<sup>−/−</sup> mice were provided by G. Pei (Tongji University, Shanghai, China), which were all with C57BL/6J genetic background. All mice were fed ad libitum, maintained at 22° to 24°C, and kept on a 12-hour light/dark cycle. All animal studies were approved by Institutional Animal Care and Use Committee of the Nanjing Medical University Experimental

Animal Department (IACUC-1811049) and carried out in compliance with the ethical regulations.

### Injection of AAVs

The AAVs, including AAV9-expressing mouse ARR1 (AAV-ARR1), mouse ARR2 siRNA (AAV-siArr2) under the F4/80 promoter, and mouse IL-4 (AAV-IL-4) or vector (AAV-NC) under the cytomegalovirus promoter, were microinjected bilaterally into C57BL/6J WT mice (male, 3 to 4 months old,  $n = 10$  in each group) at the SNc (anterior-posterior, −3.0 mm; medial-lateral,  $\pm 1.3$  mm; dorsal-ventral, −4.2 mm). The speed of injection was at 0.2  $\mu$ l/min using a stereotaxic apparatus. After 2 to 4 weeks, the mice were administered with MPTP to develop PD models. The mice were randomly assigned to each group.

### MPTP subacute PD models

MPTP-induced PD models were developed as described previously (59). Briefly, mice were administered with MPTP (20 mg/kg, subcutaneously) once a day for 5 days. After the last administration for 7 days, the mice were transcardial perfused with cold phosphate-buffered saline (PBS) or PBS plus 4% paraformaldehyde, and the brain tissues were extracted and processed for immunoblotting, RT-qPCR, immunohistochemistry, and immunofluorescence staining.

### Behavioral tests

#### Pole test

Bradykinesia and motor performance in mice were evaluated using pole test (60). All mice were placed on the top of a wooden pole (1 cm in diameter and 50 cm in height) with a 1.2-cm ball on the top and conducted preexperimental training three times. After the

training, the time required for the animals to descend to the base of the pole (total time) was counted and recorded, and 60 s was the maximum time in this test.

### Rotarod test

The rotarod test was used to evaluate the motor coordination and balance of mice (60). Briefly, mice were placed on a rotating drum with a speed of 12 rpm within 5 min to adapt. At the experiment, the rotating speed of the rotating stick was increased to 20 rpm, and the time at which the mice fell off the drum (latency time) was recorded.

### Open field test

The motor crawling speed and the autonomous behavior ability of mice were conducted using OFT (60). Mice were placed in the box with a size of 20 cm by 20 cm by 15 cm to adapt to exercise in an autonomous mobile box for 15 min before the experiment. The camera directly recorded spontaneous activities of mice in the box for a duration of 5 min, starting from the center grid. The software TopScan version 2.0 (CleverSys Inc., VA, USA) was used to quantify average crawling speed of mice (in millimeter per second). Investigators were blinded to all treatment groups in behavioral tests.

### Cell cultures and treatments

Primary microglia were prepared from neonatal mice within 3 days after birth by digestion with 0.25% trypsin/EDTA as described previously (33). The cells were suspended in complete medium [Dulbecco's modified Eagle medium (DMEM)/F-12 medium containing 1% penicillin/streptomycin and 10% fetal bovine serum (FBS)] and cultured in poly-lysine (PLL)-coated T75 flasks. The medium was changed every 3 days for 10 to 14 days. When microglia reached maturity, the flasks were shaken gently, and the cells were split onto plates precoated with PLL. After incubation with serum-free base medium for 1 hour, the cells were treated with IL-4 (20 ng/ml) for Western blotting, RT-qPCR and Seahorse XF96. The CM was collected and centrifuged at 12,000g for 10 min at 4°C, and the supernatant was used to treat neurons. Oligomycin (2 μM), rapamycin (10 nM), and MHY1485 (5 μM) were used to pretreat microglia for 1 hour before IL-4 administration according to the manufacturer's instructions and previous reports (61, 62).

BMDMs were isolated from the femur and tibia cavities of mice (male, 3 months old) and cultured in DMEM supplemented with 10% FBS, 1% streptomycin/penicillin, 1 mM sodium pyruvate, and granulocyte-macrophage colony-stimulating factor (10 ng/ml) as described (33). The medium was changed every 3 days, and the cells were used for further experiments after 7 days.

Primary cultured neurons were isolated from VM of mouse fetuses (embryonic days 15 to 16) by treatment with 0.125% trypsin/EDTA as described previously (33). The neurons were plated on PLL-coated wells and cultured in DMEM/F12 medium supplemented with 10% FBS and 1% streptomycin/penicillin for 6 hours. The media were changed to neurobasal medium supplemented with 2% B27 and 0.5 mM glutamine and half-changed every 3 days. After 6 days, neurons were treated with microglial CM (microglial CM:neurobasal = 1:2) and MPP<sup>+</sup> (30 μM) for 24 hours.

BV-2 murine microglia cells were purchased from Cell Resource Center, Institute of Basic Medical Sciences, Chinese Academy of Medical Sciences, Beijing, China and routinely grown in DMEM supplemented with 10% FBS and 1% penicillin/streptomycin at

37°C as described (63). The cells were split onto plates and treated with IL-4 (20 ng/ml) for Seahorse XF96.

### Cell transfection

siRNAs targeting ARRB1, ARRB2, and Samd4 (GenePharma, Shanghai, China) (table S2) were transfected into primary microglia and BV-2 cells using Lipofectamine RNAiMAX in Opti-MEM medium according to the manufacturer's instructions for 8 hours. After the mixture was removed, the cells were cultured in complete medium for an additional 40 hours. In overexpression experiments, the cells were transfected with ARRB1, ARRB2, and SAMD4 plasmids using Lipofectamine 3000 in Opti-MEM medium according to the manufacturer's instructions for 8 hours. After the medium was removed, the cells were cultured in complete medium for an additional 16 hours.

### Immunohistochemistry

For immunohistochemical analysis (59), frozen 25-μm-thick midbrain sections were treated with 3% H<sub>2</sub>O<sub>2</sub> for 30 min, blocked by 5% bovine serum albumin in PBS supplemented with 0.3% Triton X-100 for 60 min, and then incubated with anti-TH antibodies (1:1000) at 4°C overnight. After washing, the slides were incubated with goat anti-rabbit immunoglobulin G (H + L) and horseradish peroxidase-conjugated antibodies (1:1000) for 60 min. The TH<sup>+</sup> cells in the SNc were detected using 3,3'-diaminobenzidine staining system and imaged in a stereomicroscope (Olympus, Japan). The number of TH<sup>+</sup> cells was stereologically counted by MBF Bioscience Stereo Investigator software (MBF Bioscience, USA). Investigators were blinded to the group allocation and treatment for animal experiments when counting cells in immunohistochemistry analysis.

### Immunofluorescence staining

Immunofluorescence staining was carried out as described previously (64). Primary microglia, BMDMs, and neurons were fixed with 4% paraformaldehyde for 30 min. Frozen 25-μm-thick brain sections and fixed cells were blocked with 5% bovine serum albumin and then incubated with antibodies against CD206 (1:200), ARRB1 (1:50), ARRB2 (1:50), glial fibrillary acidic protein (1:500), Iba1 (1:500), microtubule-associated protein 2 (1:200), or Arg1 (1:50) at 4°C overnight. After washing, the slides were incubated with goat anti-rabbit Alexa Fluor 488 or anti-mouse Alexa Fluor 555 (1:500) for 1 hour and Hoechst 33324 (1:1000) for 10 min. The slides were visualized under fluorescence microscopes (Nikon TE2000-S, Melville, NY or Zeiss LSM700, Oberkochen, Germany) and analyzed by ImageJ software. Investigators were blinded to all groups in immunofluorescence analysis.

### Western blotting

Tissues or cells were lysed in radioimmunoprecipitation assay buffer containing protease inhibitor cocktail. The lysates were centrifuged at 16,000g for 15 min at 4°C, and protein concentrations in the supernatants were determined using bicinchoninic acid method according to the manufacturer's instructions. Proteins (30 μg) were separated by 8 to 12% SDS-polyacrylamide gel electrophoresis gels, transferred to polyvinylidene difluoride membranes, and detected using antibodies against ARRB1 (1:1000), ARRB2 (1:1000), CD206 (1:1000), Arg1 (1:1000), Samd4 (1:500), p-STAT6 (1:1000), STAT6 (1:1000), p-mTOR (1:1000), mTOR (1:1000), p-p70S6k (1:1000), p70S6k (1:1000), TH (1:2000), or β-actin (1:5000). After washing, the membranes were incubated with the corresponding horseradish peroxidase-conjugated

secondary antibody (1:5000) for 1 hour, and the blots were analyzed using ImageQuant LAS 4000 imaging (GE Healthcare, USA) and Bio-Rad Gel Doc XR documentation systems.

### Reverse transcription quantitative polymerase chain reaction (RT-qPCR)

Total RNA from tissues or cultured cells were extracted using TRIzol reagent, and reverse-transcribed using HiScript Q RT Super-Mix for qPCR kit according to the manufacturer's instructions. The cDNAs obtained were mixed with AceQ qPCR SYBR green master mix and gene-specific primers for RT-qPCR in a StepOnePlus instrument (Applied Biosystems, CA, USA). The cycle time values were standardized to glyceraldehyde-3-phosphate dehydrogenase of the same sample. A relative quantity was calculated using the  $2^{-\Delta\Delta CT}$  methods. The primer sequences used for qPCR were listed in table S3.

### Enzyme-linked immunosorbent assay

The concentrations of IL-10 and transforming growth factor- $\beta$  in the supernatant of BMDMs were measured using enzyme-linked immunosorbent assay kits according to the manufacturers' protocols.

### Seahorse XF96 OCR analysis

OCR in primary microglia or BV-2 cells were performed using a Seahorse XF96 Extracellular Flux Analyzer instrument as described previously (60, 65). Briefly, the cells were split on a PLL-coated 96-well polystyrene Seahorse plate in completed medium. After transfection and IL-4 stimulation, the Cell Mito Stress Test Kit was used to measure the levels of OXPHOS according to the manufacturer's instructions. Briefly, after the medium was changed to XF basal medium containing 11 mM glucose and 1% FBS, consecutive OCR measurements were performed (5 cycles per measurement) as the baseline respiratory capacity. The cells were then treated with 1  $\mu$ M oligomycin, 2  $\mu$ M carbonyl cyanide *p*-trifluoromethoxyphenylhydrazone (FCCP), 1  $\mu$ M rotenone plus 2  $\mu$ M antibiotic A, and OCR was measured as maximal respiratory capacity (5 cycles per measurement). The data were analyzed and calculated using XF Assay Result (Seahorse Wave Controller).

### Cell viability

Neurons were incubated with Cell Counting Kit-8 solution (1:10 in serum-free DMEM) at 37°C for 4 hours under darkness, and the optical absorbance at 450 nm was measured using an absorbance microplate reader (Varioskan Flash, Thermo Fisher Scientific).

### LDH release assays

The LDH release in the supernatant of neurons was measured using LDH assay kits according to the manufacturer's instructions.

### RNA sequencing

Total RNA was extracted from primary microglia with TRIzol reagent. RNA-seq libraries were prepared and sequenced on an Illumina HiSeq 4000 system by Novogene. Differential expression analyses were performed by DESeq, and the heatmap were carried out using iDEP (66).

### Statistical analysis

Statistical tests were carried out using GraphPad Prism 9.0 software. Unpaired Student's *t* test was used for comparison between two groups. One-way analysis of variance (ANOVA) or two-way repeated-measures

ANOVA was used to assess differences among multiple groups. Data are presented as the means  $\pm$  SE at least three independent experiments. Differences were considered statistically significant at \**P* < 0.05, \*\**P* < 0.01, and \*\*\**P* < 0.001.

### Supplementary Materials

**This PDF file includes:**

Figs. S1 to S10

Tables S1 to S3

Uncropped Western blots

Legend for data S1

**Other Supplementary Material for this manuscript includes the following:**

Data S1

### REFERENCES AND NOTES

- H. Ye, L. A. Robak, M. Yu, M. Cykowski, J. M. Shulman, Genetics and pathogenesis of Parkinson's syndrome. *Annu. Rev. Pathol.* **18**, 95–121 (2023).
- B. R. Bloem, M. S. Okun, C. Klein, Parkinson's disease. *Lancet* **397**, 2284–2303 (2021).
- J. Jankovic, E. K. Tan, Parkinson's disease: Etiopathogenesis and treatment. *J. Neurol. Neurosurg. Psychiatry* **91**, 795–808 (2020).
- M. G. Tansey, R. L. Wallings, M. C. Houser, M. K. Herrick, C. E. Keating, V. Joers, Inflammation and immune dysfunction in Parkinson disease. *Nat. Rev. Immunol.* **22**, 657–673 (2022).
- O. Butovsky, H. L. Weiner, Microglial signatures and their role in health and disease. *Nat. Rev. Neurosci.* **19**, 622–635 (2018).
- S. Smajić, C. A. Prada-Medina, Z. Landoulsi, J. Ghelfi, S. Delcambre, C. Dietrich, J. Jarazo, J. Henck, S. Balachandran, S. Pachchek, C. M. Morris, P. Antony, B. Timmermann, S. Sauer, S. L. Pereira, J. C. Schwamborn, P. May, A. Grünwald, M. Spielmann, Single-cell sequencing of human midbrain reveals glial activation and a Parkinson-specific neuronal state. *Brain* **145**, 964–978 (2022).
- A. J. Lee, C. Kim, S. Park, J. Joo, B. Choi, D. Yang, K. Jun, J. Eom, S.-J. Lee, S. J. Chung, R. A. Rissman, J. Chung, E. Masliah, I. Jung, Characterization of altered molecular mechanisms in Parkinson's disease through cell type-resolved multiomics analyses. *Sci. Adv.* **9**, eabo2467 (2023).
- S. Balusu, R. Prasherberger, E. Lauwers, B. De Strooper, P. Verstreken, Neurodegeneration cell per cell. *Neuron* **111**, 767–786 (2023).
- R. Feleke, R. H. Reynolds, A. M. Smith, B. Tilley, S. A. G. Taliun, J. Hardy, P. M. Matthews, S. Gentleman, D. R. Owen, M. R. Johnson, P. K. Srivastava, M. Ryten, Cross-platform transcriptional profiling identifies common and distinct molecular pathologies in Lewy body diseases. *Acta Neuropathol.* **142**, 449–474 (2021).
- X. Dong-Chen, C. Yong, X. Yang, S. Chen-Yu, P. Li-Hua, Signaling pathways in Parkinson's disease: Molecular mechanisms and therapeutic interventions. *Signal Transduct. Target. Ther.* **8**, 73 (2023).
- R. M. Ransohoff, How neuroinflammation contributes to neurodegeneration. *Science* **353**, 777–783 (2016).
- C. N. Parkhurst, G. Yang, I. Ninan, J. N. Savas, J. R. Yates, J. J. Lafaille, B. L. Hempstead, D. R. Littman, W.-B. Gan, Microglia promote learning-dependent synapse formation through brain-derived neurotrophic factor. *Cell* **155**, 1596–1609 (2013).
- J. V. Pluvineau, M. S. Haney, B. A. H. Smith, J. Sun, T. Iram, L. Bonanno, L. Li, D. P. Lee, D. W. Morgens, A. C. Yang, S. R. Shuken, D. Gate, M. Scott, P. Khatri, J. Luo, C. R. Bertozzi, M. C. Bassik, T. Wyss-Coray, CD22 blockade restores homeostatic microglial phagocytosis in ageing brains. *Nature* **568**, 187–192 (2019).
- Y. Gärtner, L. Bitar, F. Zipp, C. F. Vogelaar, Interleukin-4 as a therapeutic target. *Pharmacol. Ther.* **242**, 108348 (2023).
- J. Zhang, P. Rong, L. Zhang, H. He, T. Zhou, Y. Fan, L. Mo, Q. Zhao, Y. Han, S. Li, Y. Wang, W. Yan, H. Chen, Z. You, IL4-driven microglia modulate stress resilience through BDNF-dependent neurogenesis. *Sci. Adv.* **7**, eabb9888 (2021).
- X. Zhao, H. Wang, G. Sun, J. Zhang, N. J. Edwards, J. Aronowski, Neuronal interleukin-4 as a modulator of microglial pathways and ischemic brain damage. *J. Neurosci.* **35**, 11281–11291 (2015).
- H. J. Park, S. H. Oh, H. N. Kim, Y. J. Jung, P. H. Lee, Mesenchymal stem cells enhance  $\alpha$ -synuclein clearance via M2 microglia polarization in experimental and human parkinsonian disorder. *Acta Neuropathol.* **132**, 685–701 (2016).
- G. Casella, F. Colombo, A. Finardi, H. Descamps, G. Ill-Raga, A. Spinelli, P. Podini, M. Bastoni, G. Martino, L. Muzio, R. Furlan, Extracellular vesicles containing IL-4 modulate neuroinflammation in a mouse model of multiple sclerosis. *Mol. Ther.* **26**, 2107–2118 (2018).
- J. Xu, Z. Chen, F. Yu, H. Liu, C. Ma, D. Xie, X. Hu, R. K. Leak, S. H. Y. Chou, R. A. Stetler, Y. Shi, J. Chen, M. V. L. Bennett, G. Chen, IL-4/STAT6 signaling facilitates innate hematoma

- resolution and neurological recovery after hemorrhagic stroke in mice. *Proc. Natl. Acad. Sci. U.S.A.* **117**, 32679–32690 (2020).
20. S. Kobashi, T. Terashima, M. Katagi, Y. Nakae, J. Okano, Y. Suzuki, M. Urushitani, H. Kojima, Transplantation of M2-deviated microglia promotes recovery of motor function after spinal cord injury in mice. *Mol. Ther.* **28**, 254–265 (2020).
  21. H. Okutani, H. Yamanaka, K. Kobayashi, M. Okubo, K. Noguchi, Recombinant interleukin-4 alleviates mechanical allodynia via injury-induced interleukin-4 receptor alpha in spinal microglia in a rat model of neuropathic pain. *Glia* **66**, 1775–1787 (2018).
  22. S. Moradi, A. Zamani, M. Mazdeh, M. Ramezani, A. Komaki, E. Talebi-Ghane, M. Mahdi Eftekharian, An inclusive study on cytokine gene expression in Parkinson's disease: Advanced analysis using Bayesian regression model. *Hum. Immunol.* **84**, 123–129 (2023).
  23. M. Mogi, M. Harada, H. Narabayashi, H. Inagaki, M. Minami, T. Nagatsu, Interleukin (IL)-1 $\beta$ , IL-2, IL-4, IL-6 and transforming growth factor- $\alpha$  levels are elevated in ventricular cerebrospinal fluid in juvenile parkinsonism and Parkinson's disease. *Neurosci. Lett.* **211**, 13–16 (1996).
  24. V. V. Gurevich, E. V. Gurevich, GPCR signaling regulation: The role of GRKs and arrestins. *Front. Pharmacol.* **10**, 125 (2019).
  25. C. A. C. Moore, S. K. Milano, J. L. Benovic, Regulation of receptor trafficking by GRKs and arrestins. *Annu. Rev. Physiol.* **69**, 451–482 (2007).
  26. J. M. Martinez, A. Shen, B. Xu, A. Jovanovic, J. de Chabot, J. Zhang, Y. K. Xiang, Arrestin-dependent nuclear export of phosphodiesterase 4D promotes GPCR-induced nuclear cAMP signaling required for learning and memory. *Sci. Signal.* **16**, eade3380 (2023).
  27. J. Wess, A.-B. Oteng, O. Rivera-Gonzalez, E. V. Gurevich, V. V. Gurevich,  $\beta$ -Arrestins: Structure, function, physiology, and pharmacological perspectives. *Pharmacol. Rev.* **75**, 854–884 (2023).
  28. V. V. Gurevich, E. V. Gurevich, Plethora of functions packed into 45 kDa arrestins: Biological implications and possible therapeutic strategies. *Cell. Mol. Life Sci.* **76**, 4413–4421 (2019).
  29. A. Srivastava, B. Gupta, C. Gupta, A. K. Shukla, Emerging functional divergence of  $\beta$ -arrestin isoforms in GPCR function. *Trends Endocrinol. Metab.* **26**, 628–642 (2015).
  30. S. P. Pydi, L. F. Barella, L. Zhu, J. Meister, M. Rossi, J. Wess,  $\beta$ -Arrestins as important regulators of glucose and energy homeostasis. *Annu. Rev. Physiol.* **84**, 17–40 (2022).
  31. Y. Zhang, C. Liu, B. Wei, G. Pei, Loss of  $\beta$ -arrestin 2 exacerbates experimental autoimmune encephalomyelitis with reduced number of Foxp3<sup>+</sup> CD4<sup>+</sup> regulatory T cells. *Immunology* **140**, 430–440 (2013).
  32. Y. Shi, Y. Feng, J. Kang, C. Liu, Z. Li, D. Li, W. Cao, J. Qiu, Z. Guo, E. Bi, L. Zang, C. Lu, J. Z. Zhang, G. Pei, Critical regulation of CD4<sup>+</sup> T cell survival and autoimmunity by  $\beta$ -arrestin 1. *Nat. Immunol.* **8**, 817–824 (2007).
  33. Y. Fang, Q. Jiang, S. Li, H. Zhu, R. Xu, N. Song, X. Ding, J. Liu, M. Chen, M. Song, J. Ding, M. Lu, G. Wu, G. Hu, Opposing functions of  $\beta$ -arrestin 1 and 2 in Parkinson's disease via microglia inflammation and Nlrp3. *Cell Death Differ.* **28**, 1822–1836 (2021).
  34. Y. Xia, Z. Zhang, W. Lin, J. Yan, C. Zhu, D. Yin, S. He, Y. Su, N. Xu, R. W. Caldwell, L. Yao, Y. Chen, Modulating microglia activation prevents maternal immune activation induced schizophrenia-relevant behavior phenotypes via arginase 1 in the dentate gyrus. *Neuropsychopharmacology* **45**, 1896–1908 (2020).
  35. S. F. Enam, S. R. Kader, N. Bodkin, J. G. Lyon, M. Calhoun, C. Azrak, P. M. Tiwari, D. Vanover, H. Wang, P. J. Santangelo, R. V. Bellamkonda, Evaluation of M2-like macrophage enrichment after diffuse traumatic brain injury through transient interleukin-4 expression from engineered mesenchymal stromal cells. *J. Neuroinflammation* **17**, 197 (2020).
  36. S. Yang, C. Qin, Z.-W. Hu, L.-Q. Zhou, H.-H. Yu, M. Chen, D. B. Bosco, W. Wang, L.-J. Wu, D.-S. Tian, Microglia reprogram metabolic profiles for phenotype and function changes in central nervous system. *Neurobiol. Dis.* **152**, 105290 (2021).
  37. Z. Chen, W. Holland, J. M. Shelton, A. Ali, X. Zhan, S. Won, W. Tomisato, C. Liu, X. Li, E. M. Y. Moresco, B. Beutler, Mutation of mouse Samd4 causes leanness, myopathy, uncoupled mitochondrial respiration, and dysregulated mTORC1 signaling. *Proc. Natl. Acad. Sci. U.S.A.* **111**, 7367–7372 (2014).
  38. M. M. Mehta, S. E. Weinberg, N. S. Chandel, Mitochondrial control of immunity: Beyond ATP. *Nat. Rev. Immunol.* **17**, 608–620 (2017).
  39. E. L. Mills, B. Kelly, L. A. J. O'Neill, Mitochondria are the powerhouses of immunity. *Nat. Immunol.* **18**, 488–498 (2017).
  40. M. A. Lynch, Can the emerging field of immunometabolism provide insights into neuroinflammation? *Prog. Neurobiol.* **184**, 101719 (2020).
  41. L.-P. Bernier, E. M. York, B. A. MacVicar, Immunometabolism in the brain: How metabolism shapes microglial function. *Trends Neurosci.* **43**, 854–869 (2020).
  42. H. Yu, M. Wang, T. Zhang, L. Cao, Z. Li, Y. Du, Y. Hai, X. Gao, J. Ji, J. Wu, Dual roles of  $\beta$ -arrestin 1 in mediating cell metabolism and proliferation in gastric cancer. *Proc. Natl. Acad. Sci. U.S.A.* **119**, e2123231119 (2022).
  43. C. A. Smibert, J. E. Wilson, K. Kerr, P. M. Macdonald, smaug protein represses translation of unlocalized nanos mRNA in the *Drosophila* embryo. *Genes Dev.* **10**, 2600–2609 (1996).
  44. X.-Y. Wang, L.-N. Zhang, RNA binding protein SAMD4: Current knowledge and future perspectives. *Cell Biosci.* **13**, 21 (2023).
  45. A. J. Fernández-Alvarez, M. Gabriela Thomas, M. L. Pascual, M. Habif, J. Pimentel, A. A. Corbat, J. P. Pessoa, P. E. La Spina, L. Boscaglia, A. Plessis, M. Carmo-Fonseca, H. E. Grecco, M. Casado, G. L. Boccaccio, Smaug1 membrane-less organelles respond to AMPK and mTOR and affect mitochondrial function. *J. Cell Sci.* **135**, jcs253591 (2022).
  46. J. S. Smith, S. Rajagopal, The  $\beta$ -arrestins: Multifunctional regulators of G protein-coupled receptors. *J. Biol. Chem.* **291**, 8969–8977 (2016).
  47. L. Zhu, M. Rossi, Y. Cui, R. J. Lee, W. Sakamoto, N. A. Perry, N. M. Urs, M. G. Caron, V. V. Gurevich, G. Godlewski, G. Kunos, M. Chen, W. Chen, J. Wess, Hepatic  $\beta$ -arrestin 2 is essential for maintaining euglycemia. *J. Clin. Invest.* **127**, 2941–2945 (2017).
  48. S. Kook, X. Zhan, W. M. Cleghorn, J. L. Benovic, V. V. Gurevich, E. V. Gurevich, Caspase-cleaved arrestin-2 and BID cooperatively facilitate cytochrome C release and cell death. *Cell Death Differ.* **21**, 172–184 (2014).
  49. S. Kook, S. A. Vishnivetskiy, V. V. Gurevich, E. V. Gurevich, Cleavage of arrestin-3 by caspases attenuates cell death by precluding arrestin-dependent JNK activation. *Cell. Signal.* **54**, 161–169 (2019).
  50. R. S. Haider, E. S. F. Matthees, J. Drube, M. Reichel, U. Zabel, A. Inoue, A. Chevnigné, C. Krasel, X. Deupi, C. Hoffmann,  $\beta$ -Arrestin1 and 2 exhibit distinct phosphorylation-dependent conformations when coupling to the same GPCR in living cells. *Nat. Commun.* **13**, 5638 (2022).
  51. R. H. Oakley, J. Revollo, J. A. Cidlowski, Glucocorticoids regulate arrestin gene expression and redirect the signaling profile of G protein-coupled receptors. *Proc. Natl. Acad. Sci. U.S.A.* **109**, 17591–17596 (2012).
  52. J. Li, A. Guo, Q. Wang, Y. Li, J. Zhao, J. Lu, G. Pei, NF- $\kappa$ B directly regulates  $\beta$ -arrestin-1 expression and forms a negative feedback circuit in TNF- $\alpha$ -induced cell death. *FASEB J.* **32**, 4096–4106 (2018).
  53. J. Wang, W. Xu, T. Zhong, Z. Song, Y. Zou, Z. Ding, Q. Guo, X. Dong, W. Zou, miR-365 targets  $\beta$ -arrestin 2 to reverse morphine tolerance in rats. *Sci. Rep.* **6**, 38285 (2016).
  54. A. Kraemer, Z. Barjaktarovic, H. Sarioglu, K. Winkler, F. Eckardt-Schupp, S. Tapio, M. J. Atkinson, S. Moertl, Cell survival following radiation exposure requires miR-525-3p mediated suppression of ARRB1 and TXN1. *PLOS ONE* **8**, e77484 (2013).
  55. W. Sang, Y. Wang, C. Zhang, D. Zhang, C. Sun, M. Niu, Z. Zhang, X. Wei, B. Pan, W. Chen, D. Yan, L. Zeng, T. P. Loughran, K. Xu, MiR-150 impairs inflammatory cytokine production by targeting ARRB-2 after blocking CD28/B7 costimulatory pathway. *Immunol. Lett.* **172**, 1–10 (2016).
  56. J. Zhao, Y. Feng, H. Yan, Y. Chen, J. Wang, B. Chua, C. Stuart, D. Yin,  $\beta$ -Arrestin2/miR-155/GSK3 $\beta$  regulates transition of 5'-azacytidine-induced Sca-1-positive cells to cardiomyocytes. *J. Cell Mol. Med.* **18**, 1562–1570 (2014).
  57. D. J. Luessen, H. Sun, M. M. McGinnis, M. Hagstrom, G. Marrs, B. A. McCool, R. Chen, Acute ethanol exposure reduces serotonin receptor 1A internalization by increasing ubiquitination and degradation of  $\beta$ -arrestin2. *J. Biol. Chem.* **294**, 14068–14080 (2019).
  58. M. Golan, G. Schreiber, S. Avissar, Antidepressants increase  $\beta$ -arrestin2 ubiquitination and degradation by the proteasomal pathway in C<sub>6</sub> rat glioma cells. *J. Pharmacol. Exp. Ther.* **332**, 970–976 (2010).
  59. J. Zhu, Z. Hu, X. Han, D. Wang, Q. Jiang, J. Ding, M. Xiao, C. Wang, M. Lu, G. Hu, Dopamine D2 receptor restricts astrocytic NLRP3 inflammasome activation via enhancing the interaction of  $\beta$ -arrestin2 and NLRP3. *Cell Death Differ.* **25**, 2037–2049 (2018).
  60. N. Song, Y. Fang, H. Zhu, J. Liu, S. Jiang, S. Sun, R. Xu, J. Ding, G. Hu, M. Lu, Kir6.2 is essential to maintain neurite features by modulating PM20D1-reduced mitochondrial ATP generation. *Redox Biol.* **47**, 102168 (2021).
  61. Q. Li, Y. Zhao, H. Guo, Q. Li, C. Yan, Y. Li, S. He, N. Wang, Q. Wang, Impaired lipophagy induced-microglial lipid droplets accumulation contributes to the buildup of TREM1 in diabetes-associated cognitive impairment. *Autophagy* **19**, 2639–2656 (2023).
  62. J. Van den Bossche, J. Baardman, N. A. Otto, S. van der Velden, A. E. Neele, S. M. van den Berg, R. Luque-Martin, H.-J. Chen, M. C. S. Boshuizen, M. Ahmed, M. A. Hoeksema, A. F. de Vos, M. P. J. de Winther, Mitochondrial dysfunction prevents repolarization of inflammatory macrophages. *Cell Rep.* **17**, 684–696 (2016).
  63. Y. Fang, L. Yao, C. Li, J. Wang, J. Wang, S. Chen, X.-F. Zhou, H. Liao, The blockage of the Nogo/NgR signal pathway in microglia alleviates the formation of A $\beta$  plaques and tau phosphorylation in APP/PS1 transgenic mice. *J. Neuroinflammation* **13**, 56 (2016).
  64. Y. Fang, X. Ding, Y. Zhang, L. Cai, Y. Ge, K. Ma, R. Xu, S. Li, M. Song, H. Zhu, J. Liu, J. Ding, M. Lu, G. Hu, Fluoxetine inhibited the activation of A1 reactive astrocyte in a mouse model of major depressive disorder through astrocytic 5-HT2B/ $\beta$ -arrestin2 pathway. *J. Neuroinflammation* **19**, 23 (2022).
  65. X. Gu, Y. Ma, Y. Liu, Q. Wan, Measurement of mitochondrial respiration in adherent cells by Seahorse XF96 Cell Mito Stress Test. *STAR Protoc.* **2**, 100245 (2021).
  66. S. X. Ge, E. W. Son, R. Yao, iDEP: An integrated web application for differential expression and pathway analysis of RNA-seq data. *BMC Bioinformatics* **19**, 534 (2018).

**Acknowledgments:** We would like to thank G. Pei for providing ARRB2 KO (Arrb2<sup>-/-</sup>) mice and L. Ma for providing ARRB2 overexpression plasmid. **Funding:** The work reported herein was

supported by the grants from the National Key R&D Program of China (no. 2021ZD0202900 to G.H.), National Natural Science Foundation of China (nos. 81991523 and 81630099 to G.H. and 81703488 to Y. Fang), and Natural Science Foundation of the Basic Research Program of Jiangsu Province (no. BK20171061 to Y. Fang). **Author contributions:** Conceptualization: Y. Fang, G.H., J.L., Y. Fan, M.L. and J.D. Methodology: Y. Fang, G.H., and J.D. Investigation: J.L., Y.L., Y. Fang, Q.M., J.C., J.M., L.C., H.Z., and N.S. Validation: Y. Fang, G.H., J.L., and J.D. Visualization: J.L., Y.L., Y. Fang, and G.W. Supervision: G.H. and Y. Fang. Writing—original draft: Y. Fang, J.L., G.W., and Y.L. Writing—review and editing: G.W., Y. Fang, G.H., and J.L. Resources: G.H., Y. Fang, and J.D. Project administration: G.H. and Y. Fang. Funding acquisition: G.H. and Y. Fang. All authors

approved the final version of the manuscript. **Competing interests:** The authors declare that they have no competing interests. **Data and materials availability:** All data needed to evaluate the conclusions in the paper are present in the paper and/or the Supplementary Materials.

Submitted 12 December 2023

Accepted 17 July 2024

Published 21 August 2024

10.1126/sciadv.adn4845